Correlation effects, circular dichroism, and Fermi surfaces of bulk nickel from soft x-ray angle-resolved photoemission

J. Braun,[1] J. Minár,[1] H. Ebert,[1] A. Chainani,[2] J. Miyawaki,[2] Y. Takata,[2,*] M. Taguchi,[2] M. Oura,[2] and S. Shin[2,3]

[1]*Department Chemie/Physikalische Chemie, Ludwig-Maximilians Universität München, Munich, Germany*

[2]*RIKEN/SPring-8, Sayo-cho, Sayo-gun, Hyogo 679-5148, Japan*

[3]*Institute for Solid State Physics (ISSP), The University of Tokyo, Kashiwanoha, Kashiwa, Chiba 277-8581, Japan*

(Received 17 July 2011; revised manuscript received 24 January 2012; published 5 April 2012)

Within this soft x-ray photoemission study we present a detailed experimental and theoretical view on the bulk-related electronic structure of ferromagnetic nickel. Our results resolve the long-standing issue of the Fermi surfaces of bulk Ni and thereby establish the validity of a local correlation picture for its electronic structure. We performed complementary theoretical and experimental soft x-ray angle-resolved photomission spectroscopy studies to determine the Fermi surfaces and correlation effects in the bulk states of Ni. The electronic structure, obtained from the local-spin density approximation with dynamical mean-field theory and one-step photoemission calculations including matrix elements, is based on a fully relativistic treatment using a complex and energy-dependent self-energy $\Sigma(E)$. The experimental band dispersions, the circular dichroism in the spectral functions, and the experimentally extracted self-energy $\Sigma(E)$ are in agreement with theoretical findings.

DOI: 10.1103/PhysRevB.85.165105 PACS number(s): 73.20.−r, 75.70.Rf, 75.50.Bb, 79.60.−i

I. INTRODUCTION

Angle-resolved photoemission spectroscopy (ARPES) provides direct access to momentum- (k) and energy- (E) resolved electronic structures, and consequently allows a determination of the self-energy $\Sigma(E)$ of electronic states in the vicinity of the Fermi level (E_F) which constitute Fermi surfaces (FSs). Modern experimental setups use high flux photon sources, efficient analyzers, and detectors, and supply high k and E resolution as well as spin resolution. The resulting spectra have provided major insights in the study of new materials such as low-dimensional magnetic structures, low- and high-T_C superconductors, topological insulators, etc.[1] However, a comprehensive understanding of the underlying physics of such materials and a quantitative analysis of correlation effects requires a realistic calculation of excitation spectra. Moreover, since x-ray ARPES is now established as a powerful electronic structure method,[2–5] theoretical calculations are necessary to understand band dispersions (BDs) and intensities of the spectral features.

A first step in this direction was carried out for low-energy ARPES, covering $h\nu \sim 10$–100 eV.[6] It was shown that the experimental BDs and spectral functions of nickel are best described by calculations based on local-spin density approximation with dynamical mean-field theory (LSDA + DMFT) for the electronic structure combined with the one-step model for photoemission intensities including matrix elements. The detailed comparison of energy distribution curves (EDCs) provided a good description but also suggested the influence from surface effects due to the small mean free path of the emitted electrons. To clarify this issue, polarization-dependent soft x-ray (SX)-ARPES with $h\nu \sim 400$–800 eV has been carried out.[2–5,7–9] Within a theoretical SX-ARPES approach, which was recently developed and applied to Ag(001) (Ref. 8) and W(110),[9] we present a detailed comparison with experimental band maps, EDCs, and FSs of bulk ferromagnetic Ni(001), the prototype of moderate electron-electron correlations.

Nickel metal has been extensively studied using angle-integrated x-ray and resonant PES,[10–13] as well as low-energy ARPES and theory.[6,14–23] The salient features of its electronic structure indicate that (a) the experimental bandwidths are reduced by about 30% compared to LSDA results,[14] (b) the spectra show a dispersionless feature at about 6 eV binding energy (BE), namely, the so-called two-hole correlation satellite, and (c) the magnetic exchange splitting between up- and down-spin bands is ∼250–300 meV. Early studies implicated electron-electron correlations as the cause of the band narrowing and the correlation satellite.[10–12] More recently, the validity of LSDA-calculated BDs and FSs in relation with the experimental results has been debated in the literature. Bunemann *et al*. proposed that correlations modify the dispersion of the $\Delta_{2\downarrow}$ band to the extent that it does not cross E_F, and accordingly the associated $X_{2\downarrow}$ FS sheet is missing,[15] and analyzed in a second study the role of spin-orbit coupling on the FS topology using the LDA + Gutzwiller scheme in combination with a parametrized spin-orbit Hamiltonian.[24] Varykhalov *et al*.[16] and Cui *et al*.[17] concluded the importance of final-state effects in low-energy ARPES of Ni within a LSDA picture. Based on LSDA theory, Sahrakorpi *et al*. showed[18] that, for low-energy ARPES of Ni(001), a three-step model calculation (i.e., taking into account excitation, transport, and ejection of the photoelectron as separate processes) yielded similar conclusions as a one-step model calculation while recognizing the role of initial- and final-state effects. Hofmann *et al*.[19] probed quasiparticle dynamics and identified a correlation-induced kink at ∼0.3 eV in the dispersion of the bulk magnetic bands of Ni(110). Kamakura *et al*.[7] reported a SX-ARPES study and concluded consistency of the FSs with LSDA results, but did not report a quantitative analysis of the BDs and spectral intensities. Very recent studies[20,21] on 1–6 monolayer films of Ni/Cu(100) have shown two- and three-dimensional BDs and FSs, while a spin-resolved ARPES study[22] showed spin-split surface states of Ni(111) with a reduced exchange splitting of 55–160 meV. In a low-energy ARPES study, Braun *et al*.[6] showed that the spectral intensities

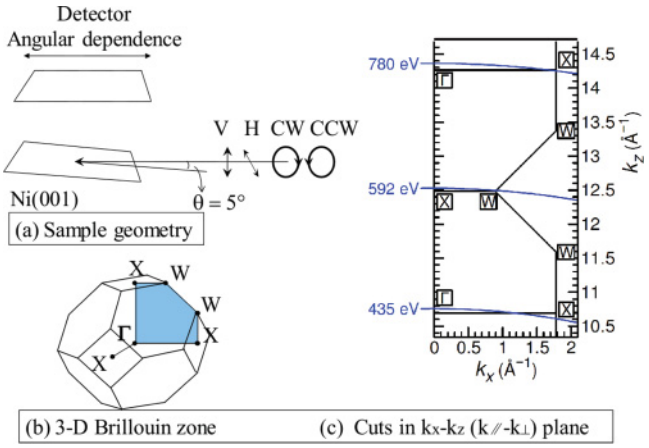

FIG. 1. (Color online) (a) Experimental geometry adopted to measure the polarization-dependent SX-ARPES. (b) Three-dimensional Brillouin zone of Ni metal. (c) Energy-dependent cuts in the k_x-k_z plane, which were measured in order to accurately determine the momentum values for the SX-ARPES experiments.

calculated within the one-step model using LSDA + DMFT calculations best describe the electronic structure of Ni. The calculated FSs and BDs reported by LSDA + DMFT have also discussed the role of correlations in relation to the $\Delta_{2\downarrow}$ band and the associated $X_{2\downarrow}$ FS. While Yang *et al.*[23] concluded that the $X_{2\downarrow}$ FS is missing because the occupied $\Delta_{2\downarrow}$ BD gets shifted to higher BEs, i.e., away from E_F, Braun *et al.*[6] showed that the BDs are shifted to lower BEs, i.e., toward E_F. In order to resolve these issues, we have carried out polarization-dependent SX-ARPES experiments and corresponding calculations.

II. EXPERIMENTAL AND CALCULATIONAL DETAILS

The electronic structure has been calculated within the framework of the fully relativistic Korringa-Kohn-Rostoker multiple-scattering theory (SPRKKR).[25] To account properly for electronic correlations beyond the LSDA,[26,27] we use a complex and energy-dependent self-energy $\Sigma(E)$,[28] which is determined by a self-consistent LSDA + DMFT calculation.[6] The most successful theoretical approach to PES and inverse photoemission (IPE) is the so-called one-step model of photoemission as originally proposed by Pendry and co-workers.[29] Due to the high excitation energies, a special treatment of the final state is essential within our study because the multiple scattering is more or less reduced to single-scattering events.[8,9] SX-ARPES experiments were carried out on a bulk single crystal of Ni(001) at beamline BL17SU of SPring-8, and the complete experimental details are described in Ref. 7. Figures 1(a)–1(c) show the experimental geometry, the Brillouin zone (BZ) of bulk Ni, and the cuts in the k_x-k_z plane that were measured to accurately determine the momentum values in the Brillouin zone.

All measurements reported here were carried out at $T = 50$ K to minimize indirect transitions which are known to cause band smearing.[7–9,30] Figure 2 shows the (a) experimental and (b) calculated SX-ARPES spectral intensity band maps for circular polarization and $h\nu = 435$ eV, which probe the Γ-X cut in the BZ of Ni (see Fig. 1). As usual, the self-energy within the DMFT is parametrized by the averaged screened Coulomb interaction U and the exchange interaction J. For the ferromagnetic $3d$ transition metals Fe, Co, and Ni it is usually accepted that the averaged on-site exchange interaction J coincidences with its atomic value $J \approx 0.9$ eV. This parameter can be calculated directly within the LSDA and is approximately the same for all $3d$ elements.[31] For the parameter U, semiempirical values are usually used[32,33] and are estimated to be between 1 and 3 eV. In our theoretical analysis, we used the values $U = 2.8$ eV and $J = 0.9$ eV for the average screened Coulomb interaction U and the exchange interaction J. With these values we found an optimal agreement between the experimental and theoretical peak positions. This was also shown in an earlier study.[6] To take account of impurity

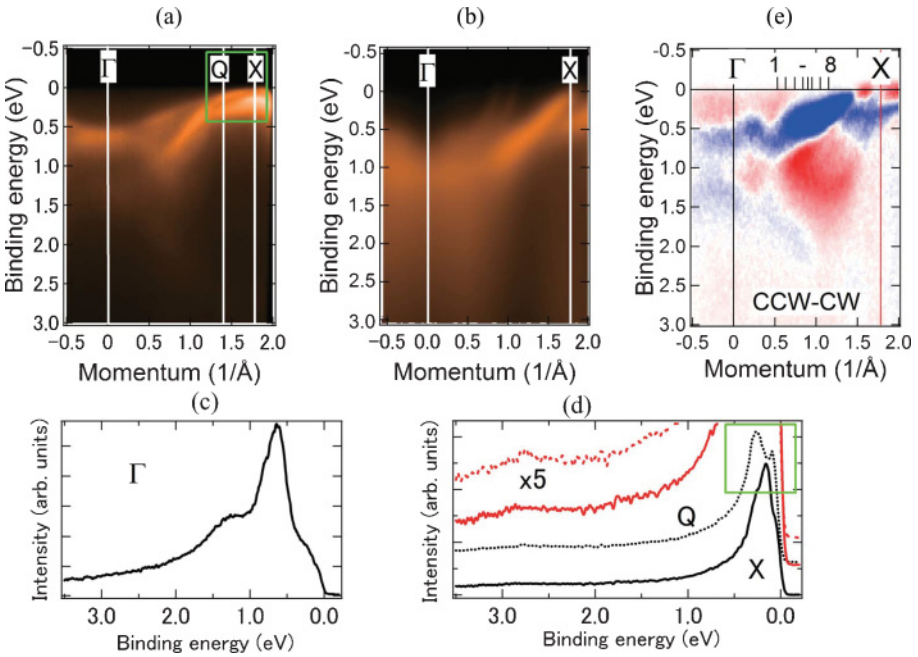

FIG. 2. (Color online) (a) Experimental and (b) calculated SX-ARPES spectral intensity band maps for circular polarization of incident soft x rays with energy $h\nu = 435$ eV, which probe the Γ-X cut in the BZ of Ni (see Fig. 1). (c) The EDC at the Γ point. (d) The EDCs at the Q and X points, along with a five times magnification which shows the weak $\Delta_{2'}$ band at nearly 3-eV BE. Experimental SX-ARPES circular dichroism [counter-clockwise (CCW)-clockwise(CW)] band map for soft x rays with $h\nu = 435$ eV, showing a dichroism change near the X point.

scattering, we added a small constant value of 0.05 eV to the imaginary part of the complex $\Sigma(E)$. For the final state, a constant imaginary value $V_f = 5.0$ eV has been chosen in a phenomenological way.[8,9]

III. RESULTS

The Γ-X cut band map of Fig. 2(a) at first glance looks similar to that of Kamakura *et al.*,[7] which reported band maps up to 2-eV BE using horizontal and vertical polarization. However, the present SX-ARPES study using circular polarization (ranging up to higher BEs of about 4 eV, and with higher-energy resolution) reveal significant differences. In order to see these differences more clearly, we have also plotted the experimental band maps together with the calculated band dispersions in Fig. 3. Figure 3(a) shows the calculated band dispersions overlaid on the raw experimental intensity map. The raw data is plotted on a false color scale to highlight the overall bandwidths of intense features at binding energies of 0–1.5 eV as well as the weak $\Delta_{2'}$ band (white circles mark the peak positions). The $\Delta_{2'}$ band is also seen as a weak peak in the EDCs at about 3-eV binding energy, as plotted on an expanded scale (5×) in Fig. 2(d). In Fig. 3(b), we plot the derivative map to highlight the actual band dispersions compared to the calculations. While the band dispersions show small discrepancies and do not match perfectly with the calculations [e.g., Fig. 3(b) for the $\Delta_{2\downarrow}$ band crossing near the X point does not match perfectly], the overall bandwidths and positions are better reproduced in LSDA + DMFT compared to earlier LSDA results.[6] The white squares mark the peak positions estimated from peak fits discussed later in Fig. 5. The band assignments are accordingly labeled for the calculated band dispersions.

These results allow us to distinguish between LSDA and LSDA + DMFT results, based on the following important features: (i) At the Γ point, as seen in the experimental and calculated maps [Figs. 2(a) and 2(b)], the feature centered at 0.7-eV BE originates in the Δ_1 and Δ_2 bands while the feature at 1.0–1.5 eV BE is due to the $\Delta_{2'}$ and Δ_5 bands. This matches the fully relativistic calculated band dispersions using LSDA + DMFT.[6] As is clear from the results, there is no other band present at higher BEs at the Γ point. This is seen in the EDC at the Γ point shown in Fig. 2(c). In LSDA calculations, the $\Delta_{1,2}$ and $\Delta_{2',5}$ derived features are expected at 1.2- and 2.2-eV BE, respectively, while LSDA + DMFT calculations[6] have shown that they get shifted to lower BEs (∼0.7 and 1.5 eV, respectively), as observed in the experiment. (ii) Although the present experiments are spin integrated, the calculated maps allow for an assignment of the experimental bands in terms of their spin-projected character. Figures 3(a) and 3(b) clearly show that not only the $\Delta_{5\downarrow\uparrow}$ bands but an additional band (identified as the $\Delta_{2\downarrow}$ band) also crosses E_F at a momentum value of ∼0.9 times (Γ-X). Consequently, at the X point, only the $\Delta_{2\uparrow}$ band is observed at a BE of 0.2 eV below E_F [Figs. 2(a), 2(b), and 2(d)]. In LSDA results two bands (the $\Delta_{2\uparrow}$ and $\Delta_{5\uparrow}$ bands) are expected within 0.5-eV BE at the X point. The band maps show that just before the X point is reached [white line labeled Q)], we see evidence for two bands near E_F, but the $\Delta_{2\downarrow}$ band crosses E_F just before the X point is reached, leaving only the $\Delta_{2\uparrow}$ band below E_F. This is also seen from the EDCs at the X and Q points shown in Fig. 2(d). To the best of our knowledge, this behavior has not been reported to date and we attribute the higher depth sensitivity of soft x rays and an energy resolution of ∼60 meV at $h\nu = 435$ eV for this observation. More interestingly, a clear switching of the circular dichroism (CD) was observed for the crossing associated with the $\Delta_{2\downarrow}$ compared to the $\Delta_{5\downarrow\uparrow}$ bands [Fig. 2(e)], and is discussed in the following.

Figure 2(e) shows the experimental circular dichroism map for the Γ-X cut. The experimental map is obtained as the difference in the counterclockwise (CCW) and clockwise (CW) spectral intensities measured using $h\nu = 435$ eV and an energy resolution of about 100 meV. A set of EDCs showing the dichroism for momenta labeled 1–8 in Fig. 2(e), along with corresponding calculations, is shown in Figs. 4(a) and 4(b), respectively. Figures 4(a) and 4(b) indicate that the dichroism is similar to an early low-energy ($h\nu = 11$–27 eV) spin-integrated ARPES study which investigated the magnetic dichroism.[34,35] The dichroism was attributed to a combination of the magnetic exchange splitting (∼300 meV) and spin-orbit

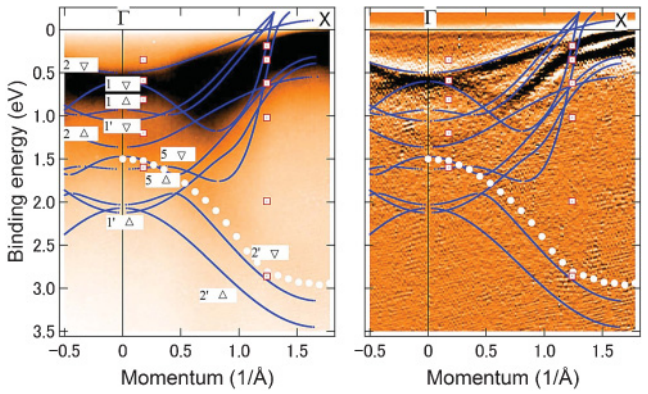

FIG. 3. (Color online) (a) Comparison of the experimental map and theoretical band dispersions with the band assignments labeled for the Γ-X cut, plotted on a false color scale. (b) Comparison of the theoretical band dispersions with the derivative of the map shown in (a). The white circles mark the weak $\Delta_{2'}$ band, and the white squares mark the peak positions estimated from peak fits shown in Fig. 5.

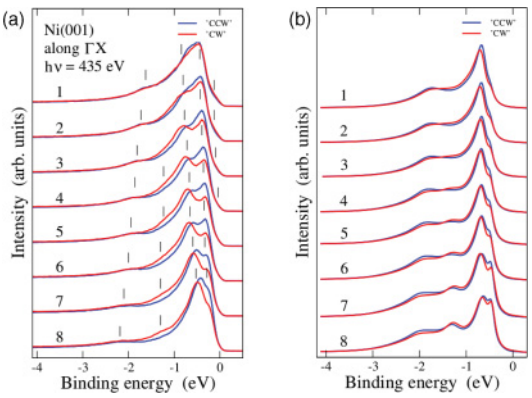

FIG. 4. (Color online) (a) Experimental and (b) calculated EDCs showing circular dichroism for momenta labeled 1–8 in Fig. 2(e) along the Γ-X cut, obtained using clockwise and counterclockwise polarization of incident photons.

splitting (∼100 meV) within a LSDA picture. While the low-energy study was carried out for magnetized Ni thin films, our experiments are carried out on bulk Ni metal without magnetizing the sample. Nevertheless, the dichroism map shown in Fig. 2(e) allows us to distinguish the E_F crossings associated with the $\Delta_{2\downarrow}$ and the $\Delta_{5\uparrow}$ bands in the form of dichroism switching at E_F around 0.9 (Γ-X), while the $\Delta_{2\uparrow}$ band alone remains below E_F at the X point as discussed above.

The band crossings and related dichroism changes are also seen in EDCs along Γ-X. In Fig. 4(a), EDC 1 shows a weak feature at 0.2 eV, strong features at 0.6 and 0.9 eV, and another weak feature at 1.8 eV. These bands disperse, as shown by tick marks in Fig. 4(a). The feature at 0.2 eV crosses the Fermi level (E_F) and is not seen in EDC 5. Similarly, the feature at 0.6 eV crosses the E_F and is not seen in EDC 8. These observations are also confirmed by the calculations as seen in Fig. 4(b). A change in the dichroism indicates a change in the dominant band character at E_F. Thus the observed FS crossing at EDC 5 and the $\Delta_{2\downarrow}$ band crossing just before the X point shows a direct relation with the switching in the CD map of Fig. 4(a), thus confirming its validity. Furthermore, the results indicate that the experimental SX-ARPES dichroism is consistent with LSDA + DMFT results of the electronic structure. The dichroic effects are caused by the interplay between the magnetic coupling terms which appear in the spin-polarized Dirac equation and the relativistic dipole selection rules.[36] The spin-orbit coupling results in hybridization gaps or avoided crossings in the fully relativistic band structure and causes a corresponding change in the effective-spin character (strictly speaking, in the presence of spin-orbit coupling, pure spin is no longer a good quantum number).[34,37] This manifests as dichroic switching along Γ-X direction, as seen in Fig. 2(e).

Next, we address the experimental imaginary part of the self-energy Im $\Sigma(E)$ for Ni metal. Figures 5(a)–5(c) show examples of fits to the EDCs along Γ-X, using Voigt functions. From such fits, we extract the experimentally measured full widths at half maxima (FWHM) of the peaks [Fig. 5(d)], which are proportional to the Im $\Sigma(E)$. Since our experiments are spin integrated and the resolution is also not high, we have used a multiple peak fitting procedure corresponding to the observed features in the data. Figure 5(d) is a compilation of data points obtained by analyzing 20 different EDCs extracted from the Γ-X band map, and three examples are shown in Figs. 5(a)–5(c). The white squares in Figs. 3(a) and 3(b) correspond to the peak positions estimated from the fitting shown in Figs. 5(a) and 5(b). Since the peak separations were found to be larger than the energy separation corresponding to the spin splitting for Ni metal (∼300 meV), known from earlier low-energy spin-resolved experiments, it indicates that we cannot unambiguously assign spin splitting in the bands. By comparing with the LSDA + DMFT calculations (Fig. 3), it is noted that the assumed peaks are always lesser in number than the expected peaks from calculations. For example, while we expect ten peaks from theory (Fig. 3), for $k_x = 0.1$ (Γ-X), we have used five peaks for the fitting [Fig. 5(a)], and for $k_x = 0.7$ (Γ-X), we have used six peaks for the fitting [Fig. 5(b)]. This leads to the situation that the estimated FWHM of peak widths at low binding energies up to 4 eV are overestimated in Fig. 5(d). Besides the experimental difficulties in estimating the self-energies, a

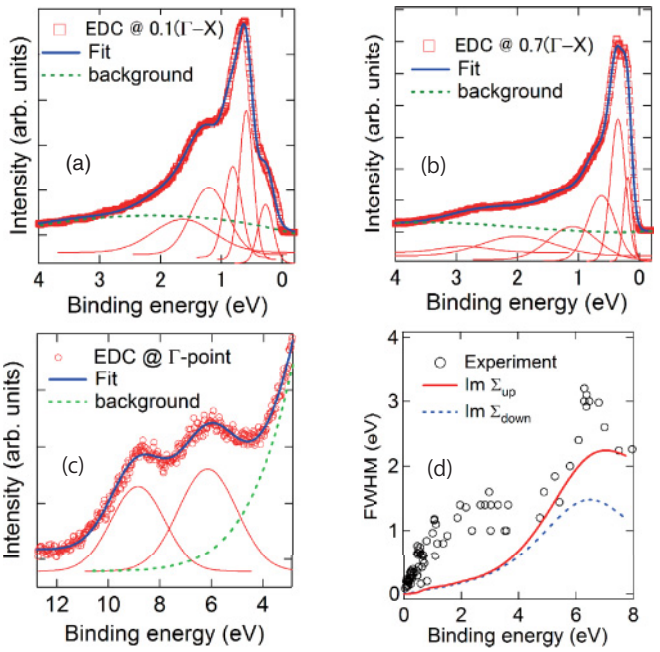

FIG. 5. (Color online) (a)–(c) Fits to EDCs along Γ-X, using Voigt functions. (d) The extracted full widths at half maxima of the peaks, which are proportional to the experimental Im $\Sigma(E)$, plotted along with the calculated Im $\Sigma(E)$.

theoretical explanation is found in terms of the many-body solver that we used in our theoretical analysis. The so-called spin-polarized T-matrix plus fluctuation exchange (SPTF) approximation[38] is of perturbational nature compared to a quantum Monte Carlo solver, which is able to consider the complete diagrammatic expansion of the self-energy in a statistical way. As a consequence, the energy dependence of the self-energy is weaker by approximately a factor of 2, and which results in an increased lifetime of the states when compared to the experiment. Nonetheless, the experimental Im $\Sigma(E)$ trend closely follows the calculated Im $\Sigma(E)$, also plotted in Fig. 5(d). Our calculated results are quite similar to an earlier report of LSDA + DMFT calculations.[33] Again, although our experiments are not spin resolved, the obtained Im $\Sigma(E)$ profiles indicate a separation of the minority and majority states in terms of their energy widths for BEs up to ∼4 eV, while the peak in Im $\Sigma(E)$ at ∼6-eV BE is due to the correlation satellite. This behavior matches fairly with our calculated Im $\Sigma(E)$, although due to the perturbational nature of the many-body solver the satellite structure appears in the theoretical density-of-states calculations at a slightly higher binding energy of about 7.2 eV compared to the experimental data. Besides these small deviations between experiment and theory, the agreement is satisfying.

Finally, in Fig. 6(a) we show the experimentally obtained FSs in the k_x-k_y plane measured using circularly polarized photons of $h\nu = 435$ eV. Band maps were obtained by tilting the sample so as to map out the FSs in the k_x-k_y plane. An energy window of 100 meV was used to determine the momentum distribution curves (MDCs) which constitute the FS map. The LSDA and LSDA + DMFT calculated FSs obtained from spectral intensities for circularly polarized x rays of $h\nu = 435$ eV are shown in Fig. 6(b). The results show

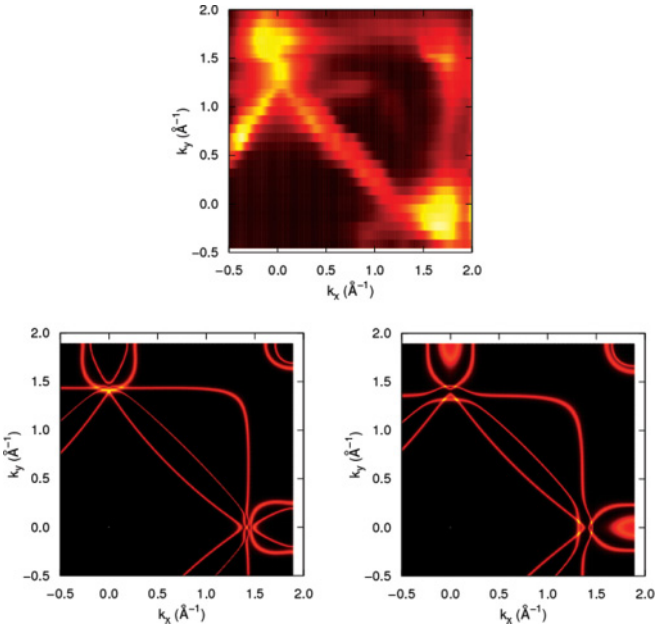

FIG. 6. (Color online) (a) The experimental FS in the k_x-k_y plane obtained from angle-dependent SX-ARPES band maps using $h\nu =$ 435 eV circularly polarized photons with $\overline{\Gamma}$ at (0,0) and $\overline{X}$ at (0,1.73). An energy window of 100 meV at E_F was used to obtain the MDCs which make up the FS map. (b) Theoretical FS maps from LSDA (left panel) and LSDA + DMFT calculations (right panel) indicate a quantitative match with the experiment.

very good consistency between experiment and theory, thus confirming the $X_{2\downarrow}$ FS in bulk Ni metal. The spectral function shown in Ref. 24 is in full agreement with our result shown in Fig. 4 as well as with the result obtained by Bünemann *et al.* in 2008. To be able to obtain the correct dispersion behavior in the vicinity of the X point, both spin-orbit interaction and many-body techniques beyond the LDA picture are necessary. In Ref. 24 the authors used the LSDA + U scheme as the static limit of a LSDA + DMFT calculation and they introduced spin-orbit interaction in a perturbational sense. We used a fully relativistic scheme in combination with a self-consistent LSDA + DMFT approach, respecting dynamical correlations and relativistic effects in a more unified picture. From this calculation we found in comparison with Ref. 24 a slightly modified behavior in the dispersion of the second band. This band now touches the Fermi level but no crossing is observed, in agreement with Bunemann *et al.*[24] Due to dynamical correlations it is smeared out and as a consequence it appears as a dot at the X point. It should be noted that such a smearing that appears just at the Fermi level should be interpreted from the experimental point of view as a second band crossing. Lastly, the FS crossings along the X-W cut measured by tilting the sample were independently confirmed by equivalent k-point measurements using circularly polarized x rays of $h\nu = 592$ eV.

IV. CONCLUSIONS

In conclusion, the overall results indeed establish the validity of LSDA + DMFT for BDs which get shifted closer to E_F. The observed circular dichroism in spectral functions, the dichroism switching, and the energy dependence of $\Sigma(E)$ including the peak structure due to the correlation satellite are consistent with LSDA + DMFT theory. The results help to resolve the long-standing issue of the Fermi surfaces of bulk Ni and confirms that nonlocal correlations are not important for Ni in contrast to Fe and Co.[33,39–41]

ACKNOWLEDGMENTS

Financial support from the Deutsche Forschungsgemeinschaft is gratefully acknowledged. The synchrotron radiation experiments (Proposal No. 20090040) were performed with the approval of RIKEN. This work was supported by the Deutsche Forschungsgemeinschaft (Grants No. EBE-154/18 and No. FOR1346) and the Bundesministerium für Bildung und Forschung (Grants No. 05KI0WW1/2 and No. 05KSI-WMB/1).

*Deceased.

[1] A. Dallmeyer, C. Carbone, W. Eberhardt, C. Pampuch, O. Rader, W. Gudat, P. Gambardella, and K. Kern, Phys. Rev. B **61**, 5133 (2000); F. Reinert, G. Nicolay, B. Eltner, D. Ehm, S. Schmidt, S. Hüfner, U. Probst, and E. Bucher, Phys. Rev. Lett. **85**, 3930 (2000); A. Damascelli, Z. Hussain, and Z.-X. Shen, Rev. Mod. Phys. **75**, 473 (2003); T. Kiss, F. Kanetaka, T. Yokoya, T. Shimojima, K. Kanai, S. Shin, Y. Onuki, T. Togashi, C. Zhang, C. T. Chen, and S. Watanabe, Phys. Rev. Lett. **94**, 057001 (2005); D. Hsieh, Y. Xia, L. Wray, D. Qian, A. Pal, J. H. Dil, J. Osterwalder, F. Meier, G. Bihlmayer, C. L. Kane, Y. S. Hor, R. J. Cava, and M. Z. Hasan, Science **323**, 919 (2009).

[2] T. Claesson, M. Mansson, C. Dallera, F. Venturini, C. De Nadai, N. B. Brookes, and O. Tjernberg, Phys. Rev. Lett. **93**, 136402 (2004); M. Mansson, T. Claesson, M. Finazzi, C. Dallera, N. B. Brookes, and O. Tjernberg, *ibid.* **101**, 226404 (2008).

[3] S. K. Mo, H. D. Kim, J. D. Denlinger, J. W. Allen, J. H. Park, A. Sekiyama, A. Yamasaki, S. Suga, Y. Saitoh, T. Muro, and P. Metcalf, Phys. Rev. B **74**, 165101 (2006).

[4] M. Yano, A. Sekiyama, H. Fujiwara, T. Saita, S. Imada, T. Muro, Y. Onuki, and S. Suga, Phys. Rev. Lett. **98**, 036405 (2007).

[5] S. I. Fujimori, Y. Saitoh, T. Okane, A. Fujimori, H. Yamagami, Y. Haga, E. Yamamoto, and Y. Onuki, Nat. Phys. **3**, 618 (2007).

[6] J. Braun, J. Minár, H. Ebert, M. I. Katsnelson, and A. I. Lichtenstein, Phys. Rev. Lett. **97**, 227601 (2006).

[7] N. Kamakura, Y. Takata, T. Tokushima, Y. Harada, A. Chainani, K. Kobayashi, and S. Shin, Phys. Rev. B **74**, 045127 (2006).

[8] F. Venturini, J. Minár, J. Braun, H. Ebert, and N. B. Brookes, Phys. Rev. B **77**, 045126 (2008).

[9] L. Plucinski, J. Minár, B. C. Sell, J. Braun, H. Ebert, C. M. Schneider, and C. S. Fadley, Phys. Rev. B **78**, 035108 (2008).

[10]S. Hüfner, G. K. Wertheim, N. V. Smith, and M. M. Traum, Solid State Commun. **11**, 323 (1972); C. Guillot, Y. Ballu, J. Paigné, J. Lecante, K. P. Jain, P. Thiry, R. Pinchaux, Y. Pétroff, and L. M. Falicov, Phys. Rev. Lett. **39**, 1632 (1977).

[11]D. E. Eastman, F. J. Himpsel, and J. A. Knapp, Phys. Rev. Lett. **40**, 1514 (1978); F. J. Himpsel, J. A. Knapp, and D. E. Eastman, Phys. Rev. B **19**, 2919 (1979).

[12]W. Eberhardt and E. W. Plummer, Phys. Rev. B **21**, 3245 (1980).

[13]T. Greber, T. J. Kreutz, and J. Osterwalder, Phys. Rev. Lett. **79**, 4465 (1997); F. Manghi, V. Bellini, J. Osterwalder, T. J. Kreutz, P. Aebi, and C. Arcangeli, Phys. Rev. B **59**, 10409 (1999).

[14]C. S. Wang and J. Callaway, Phys. Rev. B **15**, 298 (1977).

[15]J. Bünemann, F. Gebhard, T. Ohm, R. Umstätter, S. Weiser, W. Weber, R. Claessen, D. Ehm, A. Harasawa, A. Kakizaki, A. Kimura, G. Nicolay, S. Shin, and V. N. Strocov, Europhys. Lett. **61**, 667 (2003).

[16]A. Varykhalov, A. M. Shikin, W. Gudat, P. Moras, C. Grazioli, C. Carbone, and O. Rader, Phys. Rev. Lett. **95**, 247601 (2005).

[17]X. Y. Cui, E. E. Krasovskii, V. N. Strocov, A. Hofmann, J. Schäfer, R. Claessen, and L. Patthey, Phys. Rev. B **81**, 245118 (2010).

[18]S. Sahrakorpi, M. Lindroos, and A. Bansil, Phys. Rev. B **66**, 235107 (2002).

[19]A. Hofmann, X. Y. Cui, J. Schäfer, S. Meyer, P. Höpfner, C. Blumenstein, M. Paul, L. Patthey, E. Rotenberg, J. Bünemann, F. Gebhard, T. Ohm, W. Weber, and R. Claessen, Phys. Rev. Lett. **102**, 187204 (2009).

[20]M. Hoesch, V. N. Petrov, M. Muntwiler, M. Hengsberger, J. L. Checa, T. Greber, and Jürg Osterwalder, Phys. Rev. B **79**, 155404 (2009).

[21]O. Rader, H. Wolf, W. Gudat, A. Tadich, L. Broekman, E. Huwald, R. C. G. Leckey, J. D. Riley, A. M. Shikin, F. Matsui, H. Miyata, and H. Daimon, Phys. Rev. B **79**, 245104 (2009).

[22]T. Okuda, J. Lobo-Checa, W. Auwärter, M. Morscher, M. Hoesch, V. N. Petrov, M. Hengsberger, A. Tamai, A. Dolocan, C. Cirelli, M. Corso, M. Muntwiler, M. Klöckner, M. Roos, J. Osterwalder, and T. Greber, Phys. Rev. B **80**, 180404 (2009).

[23]I. Yang, S. Y. Savrasov, and G. Kotliar, Phys. Rev. Lett. **87**, 216405 (2001).

[24]J. Bünemann, F. Gebhard, T. Ohm, S. Weiser, and W. Weber, Phys. Rev. Lett. **101**, 236404 (2008).

[25]J. Minár, L. Chioncel, A. Perlov, H. Ebert, M. I. Katsnelson, and A. I. Lichtenstein, Phys. Rev. B **72**, 045125 (2005).

[26]P. Hohenberg and W. Kohn, Phys. Rev. **136**, 864 (1964); W. Kohn and L. J. Sham, *ibid.* **140**, 1133 (1965); L. J. Sham and W. Kohn, *ibid.* **145**, 561 (1966).

[27]R. O. Jones and O. Gunnarsson, Rev. Mod. Phys. **61**, 689 (1989).

[28]G. Kotliar and D. Vollhardt, Phys. Today **57** (3), 53 (2004).

[29]J. F. L. Hopkinson, J. B. Pendry, and D. J. Titterington, Comput. Phys. Commun. **19**, 69 (1980).

[30]Z. Hussain, S. Kono, R. E. Connelly, and C. S. Fadley, Phys. Rev. Lett. **44**, 895 (1980); Z. Hussain, C. S. Fadley, S. Kono, and L. F. Wagner, Phys. Rev. B **22**, 3750 (1980).

[31]V. I. Anisimov and O. Gunnarsson, Phys. Rev. B **43**, 7570 (1991).

[32]V. I. Anisimov, F. Aryasetiawan, and A. I. Lichtenstein, J. Phys.: Condens. Matter **9**, 767 (1997).

[33]A. Grechnev, I. Di Marco, M. I. Katsnelson, A. I. Lichtenstein, J. Wills, and O. Eriksson, Phys. Rev. B **76**, 035107 (2007).

[34]W. Kuch, A. Dittschar, K. Meinel, M. Zharnikov, C. M. Schneider, J. Kirschner, J. Henk, and R. Feder, Phys. Rev. B **53**, 11621 (1996); W. Kuch and C. M. Schneider, Rep. Prog. Phys. **64**, 147 (2001).

[35]J. Henk, T. Scheunemann, S. Halilov, and R. Feder, J. Phys.: Condens. Matter **8**, 47 (1996).

[36]J. Braun, Rep. Prog. Phys. **59**, 1267 (1996).

[37]M. Pickel, A. B. Schmidt, F. Giesen, J. Braun, J. Minár, H. Ebert, M. Donath, and M. Weinelt, Phys. Rev. Lett. **101**, 066402 (2008).

[38]L. V. Pourovskii, M. I. Katsnelson, and A. I. Lichtenstein, Phys. Rev. B **72**, 115106 (2005).

[39]J. Sánchez-Barriga, J. Fink, V. Boni, I. Di Marco, J. Braun, J. Minár, A. Varykhalov, O. Rader, V. Bellini, F. Manghi, H. Ebert, M. I. Katsnelson, A. I. Lichtenstein, O. Eriksson, W. Eberhardt, and H. A. Dürr, Phys. Rev. Lett. **103**, 267203 (2009).

[40]J. Sánchez-Barriga, J. Minár, J. Braun, A. Varykhalov, V. Boni, I. Di Marco, O. Rader, V. Bellini, F. Manghi, H. Ebert, M. I. Katsnelson, A. I. Lichtenstein, O. Eriksson, W. Eberhardt, H. A. Dürr, and J. Fink, Phys. Rev. B **82**, 104414 (2010).

[41]J. Minár, J. Braun, S. Mankovsky, and H. Ebert, J. Electron. Spectrosc. Relat. Phenom. **184**, 91 (2011).